Vacuum Referred Binding Energy Scheme, Electron-Vibrational Interaction, and Energy Transfer Dynamics in $BaMg_2Si_2O_7$ Ln (Ce^{3+}, Eu^{2+}) Phosphors

Ou, Yiyi; Zhou, Weijie; Liu, Chunmeng; Lin, Litian; Brik, Mikhail G.; Dorenbos, Pieter; Tao, Ye; Liang, Hongbin

DOI
10.1021/acs.jpcc.7b12204

Publication date
2018

Document Version
Final published version

Published in
Journal of Physical Chemistry C

THE JOURNAL OF PHYSICAL CHEMISTRY C

Article

Cite This: J. Phys. Chem. C 2018, 122, 2959−2967

pubs.acs.org/JPCC

Vacuum Referred Binding Energy Scheme, Electron−Vibrational Interaction, and Energy Transfer Dynamics in $BaMg_2Si_2O_7$:Ln (Ce^{3+}, Eu^{2+}) Phosphors

Yiyi Ou,[†] Weijie Zhou,[†] Chunmeng Liu,[†] Litian Lin,[†] Mikhail G. Brik,[‡,§,∥] Pieter Dorenbos,[⊥] Ye Tao,[#] and Hongbin Liang*,[†]

[†]MOE Key Laboratory of Bioinorganic and Synthetic Chemistry, KLGHEI of Environment and Energy Chemistry, School of Chemistry, Sun Yat-sen University, Guangzhou 510275, China

[‡]College of Sciences, Chongqing University of Posts and Telecommunications, Chongqing 400065, China

[§]Institute of Physics, University of Tartu, W. Ostwald Str 1, Tartu 50411, Estonia

[∥]Institute of Physics, Jan Długosz University, Armii Krajowej 13/15, PL-42200 Częstochowa, Poland

[⊥]Faculty of Applied Sciences, Delft University of Technology, Mekelweg 15, 2629 JB Delft, The Netherlands

[#]Beijing Synchrotron Radiation Facility, Institute of High Energy Physics, Chinese Academy of Sciences, Beijing 100039, China

Supporting Information

ABSTRACT: The host structure and the synchrotron radiation VUV−UV luminescence properties of samples $BaMg_2Si_2O_7$ (BMSO):Ln (Ce^{3+}, Eu^{2+}) at different doping levels and different temperatures were investigated in detail. Three important aspects are studied to elucidate the luminescence properties of samples: (1) the vacuum referred binding energy (VRBE) scheme is constructed with the electron binding in the BMSO host bands and in the Ce^{3+} and Eu^{2+} impurity levels with the aim to explain the different thermal stabilities of Ce^{3+} and Eu^{2+} emissions; (2) the electron−vibrational interaction analysis on the narrow Eu^{2+} emission indicates a weak electron−phonon interaction in the current case; (3) by using three models (Inokuti−Hirayama, Yokota−Tanimoto, and Burshteĭn models) at different conditions, the energy transfer dynamics between Ce^{3+} and Eu^{2+} was analyzed. It reveals that the energy transfer from Ce^{3+} to Eu^{2+} via electric dipole−dipole (EDD) interaction is dominant while energy migration between Ce^{3+} is negligible. Finally, the X-ray excited luminescence spectra of samples BMSO:Ce^{3+}/Eu^{2+} are collected to evaluate their possible scintillator applications.

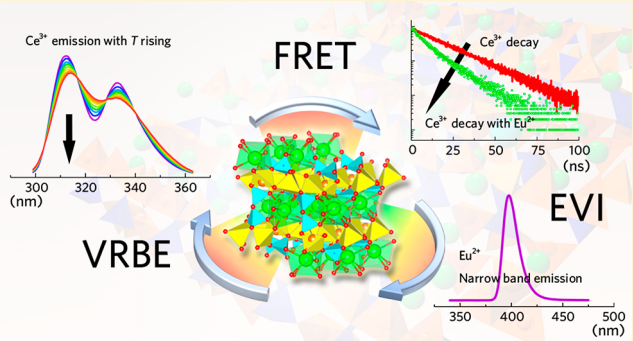

1. INTRODUCTION

Owing to their fast and tunable 5d−4f emission, Ce^{3+} and Eu^{2+} activated inorganic luminescent materials have been widely studied for applications in various fields, such as general lighting,[1−3] display,[4] ionizing radiation detection,[5] and so on. Many Ce^{3+} or Eu^{2+} activated phosphors with superior performances are commercially available. For example, Ce^{3+}-doped $Y_3Al_5O_{12}$ is a commercial yellow-emitting phosphor for white light-emitting diodes (WLEDs) excited by a blue chip, $BaMgAl_{10}O_{17}$:Eu^{2+} phosphor can provide a blue component for tricolor-based near-ultraviolet WLEDs, and Lu_2SiO_5:Ce^{3+} has been a commercial scintillator in positron emission tomography (PET) systems. Because the 4f−5d transition energies of a lanthanide ion vary in a large spectral range in different compounds, to develop the novel luminescent materials, the dependence of 4f−5d transition on host compound should be clearly and deeply understood. The construction of the vacuum referred binding energy (VRBE) scheme is a powerful tool for this aim,[6,7] and the thermal stability of these tunable emissions can also be understood by using the VRBE scheme.[8]

The electron−vibrational interaction (EVI) is another essential issue for designing novel luminescent materials with f−d transitions. Because of the participation of the outer 5d electrons, 4f−5d transitions of lanthanides are also significantly affected by the EVI process.[9] The resulting bandwidth and Stokes shift of emission bands are crucial properties that may determine their possible applications. For example, the extra-broad orange emission feature of Ce^{3+} in $Y_3Si_5N_9O$ host is caused by the strong EVI process and multiple Ce^{3+} centers, which makes this phosphor a potential component of WLEDs with high color rendering index.[10] On the contrary, the weak-

Received: December 11, 2017
Revised: January 12, 2018
Published: January 16, 2018

DOI: 10.1021/acs.jpcc.7b12204
J. Phys. Chem. C 2018, 122, 2959−2967

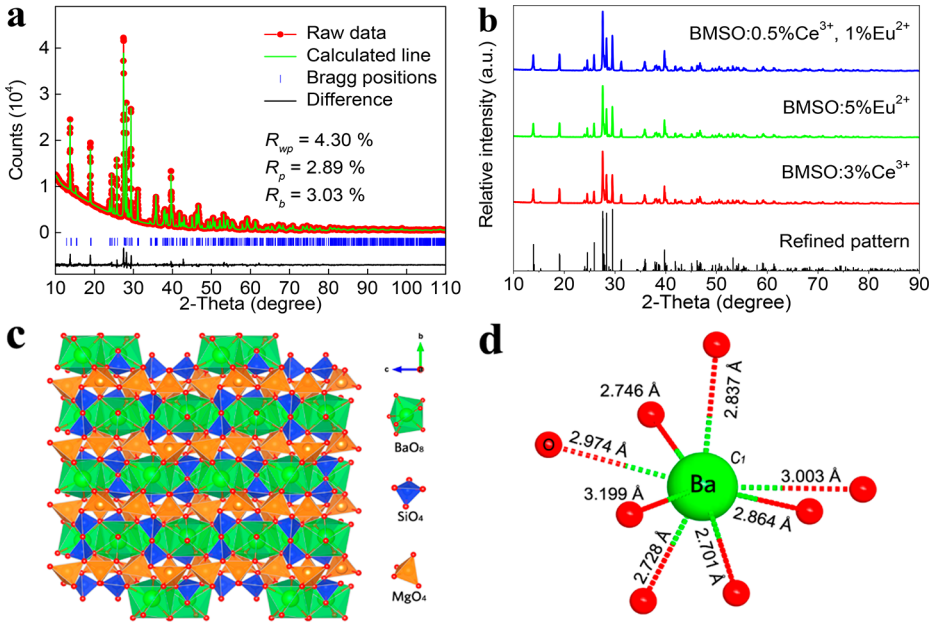

Figure 1. (a) Rietveld refinement of XRD data of $BaMg_2Si_2O_7$ at RT. (b) Representative XRD patterns of Ce^{3+}, Eu^{2+} doped samples. (c) Layered structure viewed along the *a*-axis. (d) Coordination environment of Ba^{2+} and the bond lengths between Ba^{2+} and O^{2-} ions.

EVI-induced narrow-band emission of β-SiAlON:Eu phosphor is more suitable for wide-gamut display techniques.[11]

When Ce^{3+} and Eu^{2+} are introduced into the same host lattice, Förster resonant energy transfer (FRET) may happen. The FRET process is usually utilized to achieve the sensitization of acceptor emission[12] or to fine-tune the emitting color of phosphor.[13] An efficient FRET process requires adequate spectral overlap between the donor emission and acceptor absorption, and a suitable distance between donor and acceptor, which is dependent on the type of transfer mechanism. Usually, the analysis on the donor luminescence decay properties via theoretical dynamics models is thought to be a useful method of studying the underlying energy transfer dynamics.[14]

In this paper, a series of $Ce^{3+}/Eu^{2+}/Eu^{3+}/Gd^{3+}$ singly doped and Ce^{3+}, Eu^{2+} codoped $BaMg_2Si_2O_7$ (BMSO) were prepared via a conventional solid-state reaction technique. The host structure and the VUV−UV excitation, UV−vis emission spectra, and luminescence decay curves of samples were investigated in detail. The VRBE scheme, EVI analysis, and energy transfer dynamics were studied to gain deeper insights into the luminescence properties of the samples. Finally, the X-ray excited luminescence of samples BMSO:Ce^{3+}/Eu^{2+} was collected to evaluate their possible scintillator application. The experimental section and related supporting data are presented in the Supporting Information.

2. RESULTS AND DISCUSSION

2.1. Rietveld Refinement and Crystal Structure. Figure 1a presents the Rietveld refinement of high-quality XRD data of $BaMg_2Si_2O_7$ (BMSO) at RT. The structure of $BaCo_2Si_2O_7$ (JCPDS No. 86-0770) was used as the starting model. The obtained reliability factors are R_{wp} = 4.30%, R_p = 2.89%, and R_b = 3.03%, implying a good refining quality and ensuring the phase purity. The compound BMSO crystallizes in a monoclinic structure with space group *C*2/*c*. The lattice parameters are a = 7.241 (1) Å, b = 12.71 (1) Å, c = 13.75 (1) Å, β = 90.21 (2)°, V = 1265 Å^3, and Z = 8. There are 13 crystallographic distinct ions in the unit cell, i.e., Ba^{2+}, Mg^{4+} (1−3), Si^{4+} (1, 2), and O^{2-} (1−7) (Table S1, Supporting Information). Most ions are located at Wyckoff 8f positions, except Mg1 and Mg2 at 4e positions. The Si^{4+} and Mg^{4+} all coordinate to four oxygen ions to form regular tetrahedra, which further construct the atom layers between the Ba^{2+} ions (Figure 1c). There is only one kind of Ba^{2+}site in the unit cell, which is surrounded by eight oxygen ions with C_1 point symmetry, and the average bond length is ∼2.884 Å (Figure 1d). The distance between the nearest adjacent Ba^{2+} ions is ∼4.415 Å. The XRD patterns of Ce^{3+}/Eu^{2+} singly doped and codoped BMSO samples were recorded at RT, and representative diffractograms are displayed in Figure 1b. These XRD patterns are similar and in line with the refined pattern of BMSO, indicating that all samples are of a single pure phase. Because of the similar ion radii for 8-fold coordination [Ba^{2+} (∼1.42 Å), Ce^{3+} (∼1.143 Å), Eu^{2+} (∼1.25 Å), and K^+ (∼1.51 Å)],[15] the doped Ce^{3+}, Eu^{2+} and charge compensator K^+ are expected to occupy the Ba^{2+} sites.

2.2. Luminescence of Ce^{3+} in $BaMg_2Si_2O_7$. The highest-height-normalized VUV−UV excitation (λ_{em} = 310, 323, and 332 nm) and emission (λ_{ex} = 245, 276, and 297 nm) spectra of sample $Ba_{0.990}Ce_{0.005}K_{0.005}Mg_2Si_2O_7$ (BMSO:0.5% Ce^{3+}) at 25 K are presented in Figure S1. Under different wavelength conditions, these normalized excitation and emission spectra have the same profiles within experimental error, indicating that only one kind of Ce^{3+} luminescent center is probed. Considering the host structure discussed above, this kind of Ce^{3+} luminescence is attributed to that on the Ba^{2+} site. All the excitation spectra in Figure S1 have five evident bands. The band at ∼162 nm (∼7.65 eV) is ascribed to the host exciton creation absorption, which is in line with the excitation spectrum of sample $Ba_{0.98}Gd_{0.01}K_{0.01}Mg_2Si_2O_7$ (BMSO:1% Gd^{3+}) depicted as a dashed line. Consequently, the bottom of conduction band of host compound BMSO is evaluated to be ∼8.26 eV higher than the top of the valence band when we assume that the exciton binding energy is 8% of the exciton creation energy.[16] This mobility band gap value is a somewhat

DOI: 10.1021/acs.jpcc.7b12204
J. Phys. Chem. C 2018, 122, 2959−2967

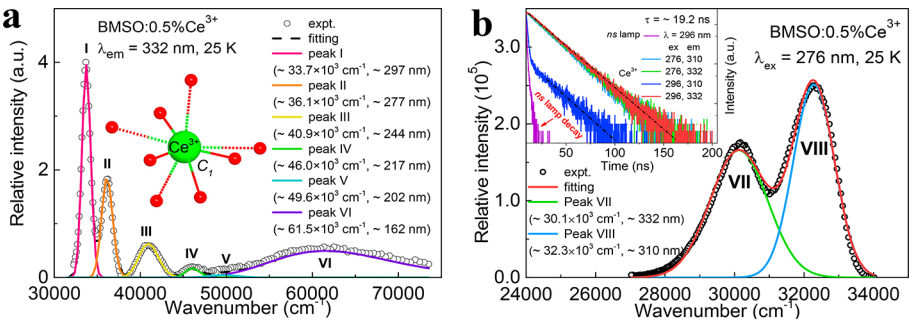

Figure 2. (a) VUV–UV excitation (λ_{em} = 332 nm) spectrum of sample BMSO:0.5% Ce^{3+} at 25 K and corresponding Gaussian fitting results. (b) Emission (λ_{ex} = 276 nm) spectrum of BMSO:0.5% Ce^{3+} at 25 K and corresponding Gaussian results. The inset shows the luminescence decay curves at RT.

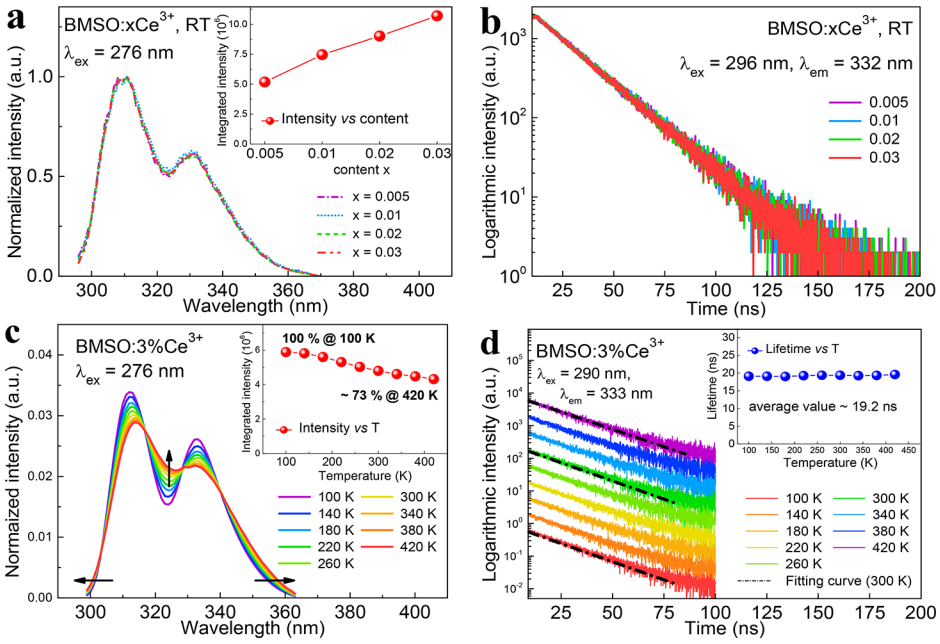

Figure 3. (a) Highest-height-normalized emission (λ_{ex} = 276 nm) spectra of BMSO:$x$$Ce^{3+}$ (x = 0.005–0.03) at RT. The inset shows the integrated emission intensity as a function of concentration. (b) Luminescence decay curves (λ_{ex} = 296 nm, λ_{em} = 332 nm) of BMSO:$x$$Ce^{3+}$ (x = 0.005–0.03) at RT. (c) Area-normalized emission (λ_{ex} = 276 nm) spectra of BMSO:3% Ce^{3+} at 100–420 K. The inset shows the integrated emission intensity as a function of temperature. (d) Luminescence decay curves (λ_{ex} = 290 nm, λ_{em} = 333 nm) of BMSO:3% Ce^{3+} at 100–420 K. The inset shows the temperature-dependent lifetime values of Ce^{3+} emission.

larger when compared to other silicates, such as Lu_2SiO_5 (~7.24 eV)[17] and $Ba_2MgSi_2O_7$ (~7.04 eV).[18] The other four evident excitation bands at ~218, ~245, ~276, and ~297 nm are attributed to the 4f → 5d transitions of Ce^{3+}. Generally, the 5d excitation band of Ce^{3+} with low point symmetry, such as C_1, will be split into five components by the crystal field. The fifth excitation band was not clearly resolved. Figure S1 also shows two bands at ~310 and ~332 nm in the emission spectra of Ce^{3+}, and they are originated to the transitions from the relaxed lowest 5d state of Ce^{3+} to 4f ground states $^2F_{5/2}$ and $^2F_{7/2}$, respectively.

To further determine the energies of the five crystal-field-split 5d excitation states of Ce^{3+} and the host absorption, the excitation (λ_{em} = 332 nm) spectrum of sample BMSO:0.5% Ce^{3+} at 25 K was fitted with a sum of six Gaussian functions (Figure 2a). The obtained bands are located at ~33.7 × 10^3 cm^{-1} (peak I), ~36.1 × 10^3 cm^{-1} (peak II), ~40.9 × 10^3 cm^{-1} (peak III), ~46.0 × 10^3 cm^{-1} (peak IV), ~49.6 × 10^3 cm^{-1} (peak V), and ~61.5 × 10^3 cm^{-1} (peak VI). Peak VI corresponds to the host exciton creation peak, which is well coincident with the result (~162 nm) discussed above. Peak V severely overlaps to the broad host exciton creation peak VI, which causes only four evident 5d excitation bands (peaks I–IV) at first glance. A similar phenomenon has been reported before in other host compounds, such as $Ba_2Ca(BO_3)_2$.[19] This peak V is tentatively assigned to the highest 5d state of Ce^{3+}, and the peaks I–IV are attributed to other four crystal-field-split 5d states. With these assignments, the centroid energy of Ce^{3+} 5d states, specifically the arithmetic mean value of five 5d states, is ~41.3 × 10^3 cm^{-1}. The difference with the free Ce^{3+} ion (51.2 × 10^3 cm^{-1}) then defines the centroid shift of ~9.9 × 10^3 cm^{-1}. In fact, the centroid shift in a compound relates to the covalence between anion ligands and 5d-orbital and anion polarizability of the anions in the first coordination sphere around Ce^{3+}. Both are closely tied to the nephelauxetic effect. The centroid shift (~9.9 × 10^3 cm^{-1}) is smaller than that of other silicates, such as Li_2CaSiO_4 (~11.6 × 10^3 cm^{-1}) and $Lu_2Si_2O_7$ (~12.4 × 10^3 cm^{-1}). This suggests a weaker covalence, spectroscopic polarizability, and nephelauxetic effect in our case.[20] The total crystal field splitting of the Ce^{3+} 5d

DOI: 10.1021/acs.jpcc.7b12204
J. Phys. Chem. C 2018, 122, 2959–2967

states is ~15.9 × 10^3 cm^{-1}. Generally, the shape and size (bond length and coordination number) of the first anion coordination polyhedron around Ce^{3+} determine the crystal field splitting.[21] Compared with other compounds with 8-fold coordination environment, the crystal field splitting of Ce^{3+} in $BaMg_2Si_2O_7$ falls between those of $BaSiO_3$ (~14.3 × 10^3 cm^{-1})[22] and $Ba_2MgSi_2O_7$ (~16.4 × 10^3 cm^{-1}).[23] Figure 2b displays the fitting results of the emission (λ_{ex} = 276 nm) spectrum by a sum of two Gaussian functions. The energies at the maxima of these two emission bands are ~30.1 × 10^3 and ~32.3 × 10^3 cm^{-1}, respectively. The Stokes shift for Ce^{3+} emission is ~1.40 × 10^3 cm^{-1}. Compared with most silicate compounds that have Stokes shift values ranging from 2000 to 3000 cm^{-1}, Ce^{3+} doped $BaMg_2Si_2O_7$ has a relatively small value. The luminescence decay curves monitoring different wavelengths are shown in the inset of Figure 2b. They are single-exponential, all with the same decay of ~19.2 ns. The fast decay component in the blue curve (λ_{ex} = 296 nm, λ_{em} = 310 nm) is from the nanosecond lamp.

Figure 3a displays the highest-height-normalized emission (λ_{ex} = 276 nm) spectra of BMSO:$x$$Ce^{3+}$ (x = 0.005−0.03) at RT. The spectral profiles and positions of these emission spectra appear identical, and the integrated emission intensity increases with increasing doping concentration as shown in the inset, indicating that no concentration quenching of Ce^{3+} emission is observed in the given concentration range (0.005−0.03). The luminescence decay curves (λ_{ex} = 296 nm, λ_{em} = 332 nm) of samples in Figure 3b confirm this view. The area-normalized emission (λ_{ex} = 276 nm) spectra of sample BMSO:3% Ce^{3+} in the temperature range of 100−420 K are shown in Figure 3c. It appears that with the increase of temperature the doublet emission peaks broaden, which is attributed to the thermal-stimulated electron−phonon interaction.[24] The integrated emission intensity in the inset drops with incremental temperature, and finally the intensity at 420 K reaches ~73% of that at 100 K. The luminescence decay curves (λ_{ex} = 290 nm, λ_{em} = 333 nm) of sample BMSO:3% Ce^{3+} are presented in Figure 3d. All the curves are single-exponential and well consistent with the fitting line of decay curve at 300 K. All the observations indicate that no evident thermal quenching of Ce^{3+} emission happens in this investigated temperature range (100−420 K). The decreasing intensity of Ce^{3+} emission with the increase of temperature may be due to the stronger self-absorption induced by thermal broadening of Ce^{3+} emission.

Generally, the thermal quenching of Ce^{3+} f−d emission is caused by the thermal ionization of 5d electrons into the conduction band. Therefore, the energy difference (E_{dc}) between the lowest 5d state and the bottom of conduction band is a measure to evaluate the luminescence thermal stability of Ce^{3+}.[25] Based on the energies of host exciton creation, Ce^{3+} centroid shift, and charge transfer band of Eu^{3+}, the vacuum referred binding energy (VRBE) scheme that links the absolute energies levels of host band structure and lanthanide ions can be constructed, and the E_{dc} value can be derived from the scheme.[26,27] In our case, the mobility band gap of host is ~8.26 eV, the centroid shift of Ce^{3+} 5d states is ~9.90 × 10^3 cm^{-1} (~1.23 eV), and the Coulomb repulsion energy U(6,A) between the Eu^{2+} and Eu^{3+} ground states is then estimated to be ~7.06 eV. The charge transfer band of Eu^{3+} is ~4.36 eV (Figure S2). Finally, the VRBE scheme for $BaMg_2Si_2O_7$ host is constructed in Figure 4, and the E_{dc} value is evaluated to be ~1.40 eV. It is larger than those of Sr_3SiO_5 (~0.88 eV)[28] and

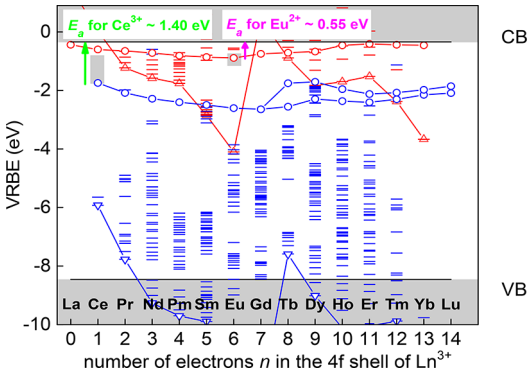

Figure 4. Vacuum referred binding energy (VRBE) scheme of lanthanide ions in $BaMg_2Si_2O_7$. The upper solid line is the bottom of conduction band (CB) while the lower one is top of valence band (VB). The blue horizontal bars, triangles, and circles represent the 4f states, 4f ground states, and lowest 5d states of Ln^{3+}, respectively. The red series are related to those of Ln^{2+}.

$Ca_2Al_2SiO_7$ (~0.59 eV),[29] which further confirms the good thermal stability of Ce^{3+} emission in $BaMg_2Si_2O_7$. From the VRBE scheme, we can also understand the thermal stability of Eu^{2+} emission as discussed below.

2.3. Luminescence of Eu^{2+} in $BaMg_2Si_2O_7$. Like the case of Ce^{3+} discussed above, there appears only one kind of Eu^{2+} luminescence originating from the Ba^{2+} site. As displayed in Figure S3, all excitation spectra monitoring emission wavelengths which cover a wavelength range of 250−400 nm have the same profiles. These are assigned to the parity allowed 4f → 5d transitions of Eu^{2+}. Under different wavelength excitations, an identical f−d emission band located at ~396 nm (~2.53 × 10^4 cm^{-1}) can also be observed in each spectrum. Its full width at half-maximum (fwhm) is only ~1457 cm^{-1} (~23 nm). This is much smaller compared to other reported oxide-based narrow-band-emitting phosphors and close to the cases of nitride-based phosphor with rigid structure and perovskite quantum dots compiled in Table S2. This narrow feature of emission band indicates a weak electron−phonon coupling in Eu^{2+} doped $BaMg_2Si_2O_7$ phosphor.[1,30] Figure 5 shows the highest-height-normalized excitation (λ_{em} = 410 nm) and emission (λ_{ex} = 350 nm) spectra of $Ba_{0.995}Eu_{0.005}Mg_2Si_2O_7$ (BMSO:0.5% Eu^{2+}) at RT in the wavenumber domain, which is consistent with the results in other works.[31] The energy of the zero-phonon line (ZPL) of Eu^{2+} transitions is estimated ~2.60 × 10^4 cm^{-1} from the intersection point between its excitation

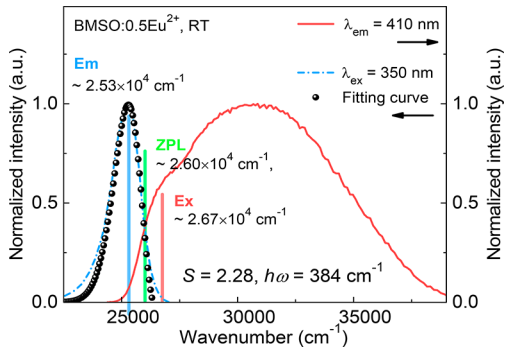

Figure 5. Highest-height-normalized excitation (λ_{em} = 410 nm) and emission (λ_{ex} = 350 nm) spectra of sample BMSO:0.5% Eu^{2+} at RT and the related fitting curve via EVI analysis.

DOI: 10.1021/acs.jpcc.7b12204
J. Phys. Chem. C 2018, 122, 2959−2967

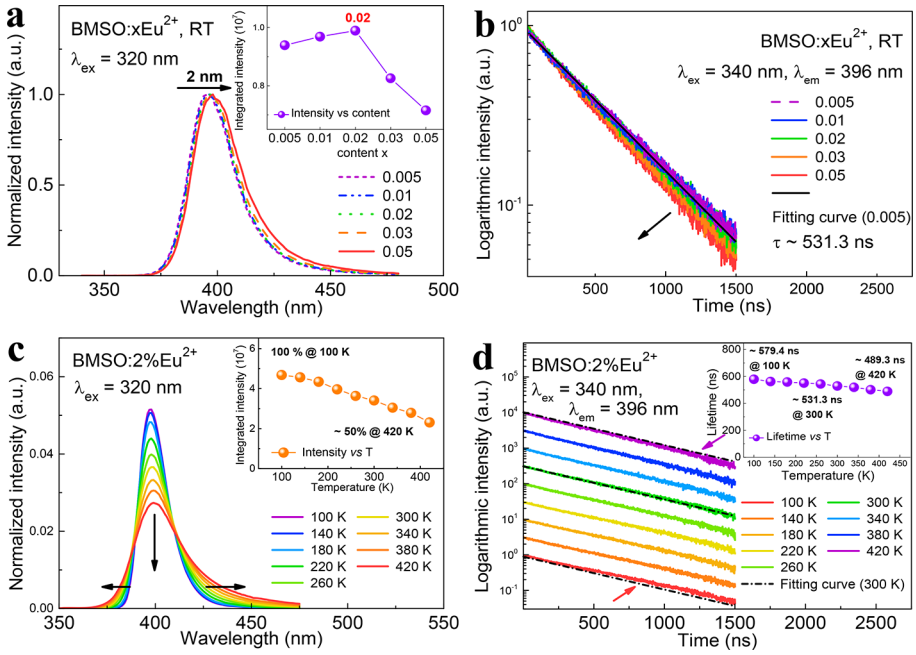

Figure 6. (a) Highest-height-normalized emission (λ_{ex} = 320 nm) spectra of BMSO:xEu^{2+} (x = 0.005−0.05) at RT. The inset shows the integrated emission intensity as a function of concentration. (b) Luminescence decay curves (λ_{ex} = 340 nm, λ_{em} = 396 nm) of BMSO:xEu^{2+} (x = 0.005−0.05) at RT. (c) Area-normalized emission (λ_{ex} = 320 nm) spectra of BMSO:2% Eu^{2+} in the temperature range 100−420 K. The inset shows the integrated emission intensity as a function of temperature. (d) Luminescence decay curves (λ_{ex} = 340 nm, λ_{em} = 396 nm) of BMSO:2% Eu^{2+} in the temperature range 100−420 K. The inset shows the average lifetime of Eu^{2+} as a function of temperature.

and emission spectra. Therefore, the energy of the relaxed lowest 5d excited state of Eu^{2+} is estimated to be ~2.67 × 10^4 cm^{-1} above the ground state. The Stokes shift of Eu^{2+} emission is ~1.37 × 10^3 cm^{-1}.

To further understand the electron−phonon coupling between Eu^{2+} and BMSO, an electron−vibrational interaction (EVI) analysis on the Eu^{2+} emission band is carried out. It is based on the Huang−Rhys theory assuming a single vibration mode with an effective vibrational frequency independent of the electronic states.[9,32] There are three main parameters describing the coupling property, i.e., the Huang−Rhys factor S, the effective phonon energy $\hbar\omega$, and the Stokes shift ΔE_S. In the framework of the single configurational coordinate model, the former two factors can be estimated by using the equations[32,33]

$$\Delta E_S = (2S - 1)\hbar\omega \tag{1}$$

$$\Gamma(T) = \sqrt{8 \ln 2}\,\hbar\omega\left[S \coth\left(\frac{\hbar\omega}{2kT}\right)\right]^{1/2} \tag{2}$$

where T is the temperature (K), k is the Boltzmann constant (6.950 × 10^{-1} (cm·K)$^{-1}$), and $\Gamma(T)$ is the full width at half-maximum (fwhm) value of the emission band at T. This value of Eu^{2+} at RT is ~1457 cm^{-1}, and the Stokes shift is ~1370 cm^{-1}. Consequently, the S and $\hbar\omega$ are calculated to be 2.28 and 384 cm^{-1}, respectively, which are similar to the results in other work.[34] Using these values, we can simulate the Eu^{2+} emission band profile via (3) to further confirm their validities.[32,33]

$$I = \frac{e^{-S}S^p}{p!}\left(1 + S^2\frac{e^{-\hbar\omega/kT}}{p+1}\right), \quad p = \frac{E_0 - E}{\hbar\omega} \tag{3}$$

where E_0 is the ZPL energy and p is the number of effective phonons involved in the coupling process between Eu^{2+} and the host compound. When E_0 is set to be ~25 960 cm^{-1}, the best simulation of Eu^{2+} emission band is achieved in Figure 5. Both the good simulation quality of emission band and coincidence between observed and simulated ZPL values confirm the validities of the obtained S and $\hbar\omega$. Compared to other cases,[35] these two parameters are smaller in our work, which gives the direct evidence for the weak coupling. Figure 6a exhibits the highest-height-normalized emission (λ_{ex} = 320 nm) spectra of BMSO:xEu^{2+} (x = 0.005−0.05) at RT. The emission band of Eu^{2+} has slight red-shift with the increase of Eu^{2+} concentration (about 2 nm from x = 0.005 to 0.5), which may relate to an increased crystal field strength and/or enhanced self-absorption at higher doping levels.[36,37] The inset shows the integrated intensity as a function of concentration. The intensity of Eu^{2+} first rises with the increase of concentration and comes to the maximum at 2 mol %. Then it decreases, which indicates the occurrence of concentration quenching. The luminescence decay curves (λ_{ex} = 340 nm, λ_{em} = 396 nm) of samples BMSO:xEu^{2+} (x = 0.005−0.05) in Figure 6b are well consistent with the view. In the diluted Eu^{2+} scenario (x = 0.005, 0.01, and 0.02), the decay lines possess the single-exponential properties with decay time of ~531.3 ns. When the concentration further increases, the decay lines remain single exponential, but the lifetime of Eu^{2+} becomes somewhat shorter, implying that another nonradiative depopulation of Eu^{2+} excited states is activated. This is attributed by an enhanced energy transfer rate (ET) between Eu^{2+} ions and excitation then finally reach killing sites, leading to energy loss of Eu^{2+} emission.[33] The internal quantum efficiencies (IQE) of these Eu^{2+} doped phosphors were measured ranging from 58% to 79% (Table S3), indicating that they are efficient. These high QE values are a requisite for light-emitting diodes (LEDs) applications.

DOI: 10.1021/acs.jpcc.7b12204
J. Phys. Chem. C 2018, 122, 2959−2967

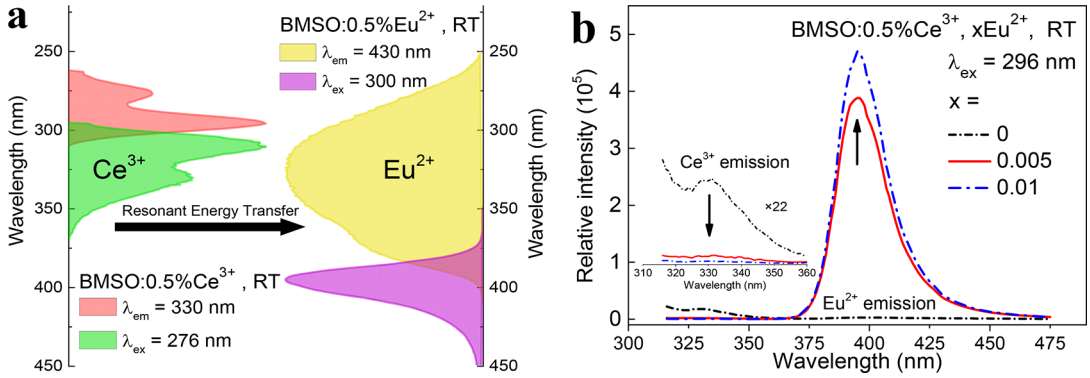

Figure 7. (a) Highest-height-normalized excitation and emission spectra of BMSO:0.5% Ce^{3+} and BMSO:0.5% Eu^{2+} at RT. (b) Emission (λ_{ex} = 296 nm) spectra of BMSO:0.5% Ce^{3+}, xEu^{2+} (x = 0−0.01) at RT; the enlargement shows the Ce^{3+} emission in the wavelength range of 316−360 nm.

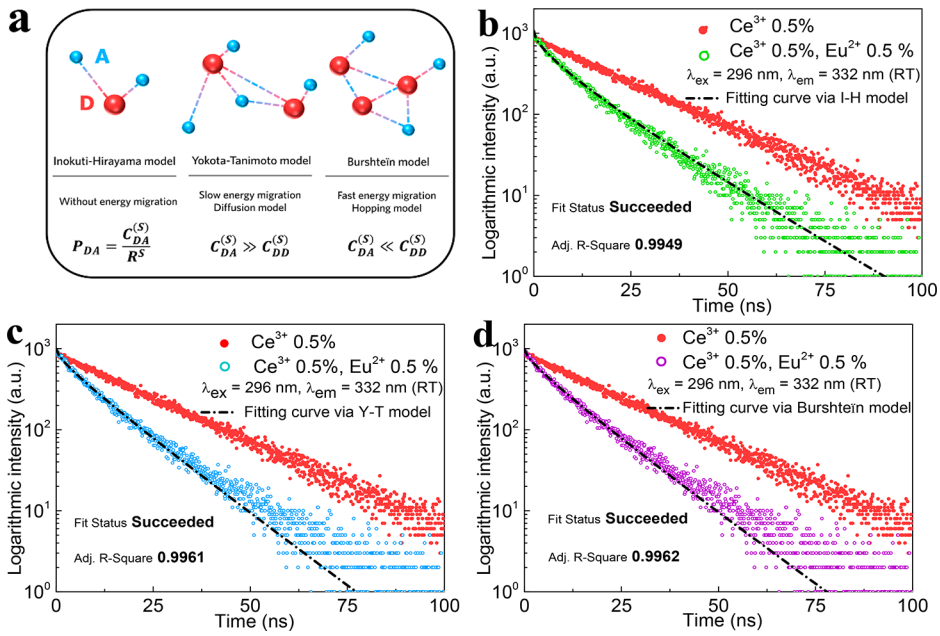

Figure 8. (a) Three different models used to analyze the luminescence decay of donor Ce^{3+}. (b, c, d) Luminescence decay curves (λ_{ex} = 296 nm, λ_{em} = 332 nm) of Ce^{3+} singly and Ce^{3+}, Eu^{2+} doubly doped samples and the related fitting results via different models.

The temperature-dependent emission (λ_{ex} = 320 nm) spectra of sample BMSO:2% Eu^{2+} under 100−420 K were collected to study the effect of temperature on luminescence of Eu^{2+}. Figure 6c exhibits the area-normalized results for clear presentation. With the increase of temperature, the Eu^{2+} emission band broadens, which is like the phenomenon of Ce^{3+}. This is also attributed to the thermal-stimulated electron−phonon interaction.[24] The less evident band broadening at the shorter wavelength side is mainly caused by the inhomogeneous broadening. The inset shows a decreasing emission intensity of Eu^{2+} with rising temperature. The intensity at 420 K is ∼50% of that at 100 K, which shows that the thermal stability of Eu^{2+} emission is inferior to that of Ce^{3+}. From the VRBE scheme constructed above, the E_{dc} value of Eu^{2+} is ∼0.55 eV, which is smaller than that of Ce^{3+} case. Figure 6d further presents the luminescence decay curves (λ_{ex} = 340 nm, λ_{em} = 396 nm) of Eu^{2+} under 100−420 K. It appears that the lifetime of Eu^{2+} emission at 100 K (∼579.4 ns) is longer than that at 300 K (∼531.3 ns). With temperature rising, the lifetime becomes shorter, and it is ∼489.3 ns at 420 K. Two main factors accounting for these phenomena are (1) the self-absorption and re-emission of Eu^{2+} ion and (2) the thermal quenching of Eu^{2+} emission. When at lower temperature, factor 1 is dominant to cause the slightly longer lifetime of Eu^{2+} emission. At higher temperature, the contribution of factor 1 may be further enhanced, but the effect of factor 2 will be more significant, finally resulting in the shortening of Eu^{2+} emission lifetime.

2.4. Energy Transfer Dynamics between Ce^{3+} and Eu^{2+}. Because of the spectral overlap between the emission band of Ce^{3+} and the excitation band of Eu^{2+} (Figure 7a), resonant energy transfer (ET) may happen from Ce^{3+} to Eu^{2+}. The emission spectra of Ce^{3+} singly and Ce^{3+}, Eu^{2+} doubly doped samples under 296 nm (the first f−d excitation band of Ce^{3+}) excitation in Figure 7b were then analyzed. For the sample BMSO:0.5% Ce^{3+}, 0.5% Eu^{2+}, the Eu^{2+} emission band at ∼396 nm is dominant. The Ce^{3+} emission at ∼335 nm compared to Ce^{3+} singly doped case undergoes a large decrease. When the concentration of Eu^{2+} increases, the intensity of Ce^{3+} emission further drops. These phenomena prove that ET from Ce^{3+} to Eu^{2+} occurs. Thus, the enhancement of Eu^{2+} emission in Figure 7b may be attributed to the collaborative contributions of sensitization by Ce^{3+} and increasing concentration of Eu^{2+}.

DOI: 10.1021/acs.jpcc.7b12204
J. Phys. Chem. C 2018, 122, 2959−2967

To further study the energy transfer dynamics from Ce^{3+} to Eu^{2+}, we collected the donor Ce^{3+} luminescence decay curve (λ_{ex} = 296 nm, λ_{em} = 332 nm) of codoped sample BMSO:0.5% Ce^{3+}, 0.5% Eu^{2+} (Figure 8). Compared to the Ce^{3+} singly doped sample with exponential decay property, the curve of codoped sample exhibits a nonexponential behavior, which indicates that the fast ET from Ce^{3+} to Eu^{2+} depopulates the Ce^{3+} excited states. There are three different models, i.e., Inokuti–Hirayama model, Yokota–Tanimoto model, and Burshteĭn model, dealing with the donor luminescence decay curves under different conditions (Figure 8a). First, when only considering the ET from Ce^{3+} to Eu^{2+} without energy migration between donor Ce^{3+} ions, the luminescence decay curve of donor Ce^{3+} can be described by Inokuti–Hirayama model[38] as follows:

$$\frac{I(t)}{I(0)} = \exp\left[-\left(\frac{t}{\tau_0}\right) - \frac{4\pi}{3}C_A\Gamma\left(1-\frac{3}{S}\right)(C_{DA})^{3/S}t^{3/S}\right] \tag{4}$$

where $I(t)$ is the luminescence intensity of Ce^{3+} at time t and $I(0)$ is the initial intensity; τ_0 is the intrinsic lifetime of donor Ce^{3+} (~19.2 ns); C_A is the acceptor Eu^{2+} concentration (3.162 × 10^{25} m^{-3}); C_{DA} is the energy transfer microparameter; $\Gamma(x)$ is the gamma function; S value implies the type of multipolar interaction [6 for electric dipole–dipole (EDD), 8 for electric dipole–quadrupole (EDQ), and 10 for electric quadrupole–quadrupole (EQQ)]. The ET probability P_{DA} is given by $P_{DA} = C_{DA}^{(S)}/R^S$, where R is the distance between ions. When $P_{DA} = 1/\tau_0$, the obtained R value is the ET critical distance R_c. The fitting results via the Inokuti–Hirayama model are shown in Figure 8b and Table 1. When S is set to be 6, the best fitting quality (R_{adj}^2 = 0.9949) can be obtained, indicating that the main mechanism for ET from Ce^{3+} to Eu^{2+} is electric dipole–dipole (EDD) interaction. The ET microparameter C_{DA} is fitted be 10.37 × 10^{-46} m^6/s. So, the R_c is about 16.5 Å, which implies an efficient ET from Ce^{3+} to Eu^{2+}.

Table 1. Concentrations of Eu^{2+} Ions (C_A), Obtained Energy Transfer Microparameters (C_{DA}), Energy Migration Microparameters (C_{DD}), and Coefficients of Determination of Fitting Procedures (R_{adj}^2) via Inokuti–Hirayama (I–H), Yokota–Tanimoto (Y–T), and Burshteĭn Models

Eu^{2+} (at. %)	C_A (10^{25} m^{-3})	C_{DA} (10^{-46} m^6/s)	C_{DD} (10^{-46} m^6/s)	R_{adj}^2
I–H model				
0.005	3.162	10.37	–	0.9949
Y–T model				
0.005	3.162	4.901	10.70	0.9961
Burshteĭn model				
0.005	3.162	3.935	25.06	0.9962

In addition, the possible energy migration processes between donor Ce^{3+} ions could be also considered to study the luminescence decay of Ce^{3+}. When a relatively long distance between Ce^{3+}, i.e., a slow energy migration case, is considered, the Yokota–Tanimoto model (diffusion model)[39,40] for EDD interaction is used to analyze the Ce^{3+} luminescence decay in our work:

$$\frac{I(t)}{I(0)} = \exp\left[-\left(\frac{t}{\tau_0}\right) - \frac{4}{3}\pi^{3/2}C_A(C_{DA})^{1/2}t^{1/2} \times \left(\frac{1+10.87x+15.50x^2}{1+8.743x}\right)^{3/4}\right] \tag{5}$$

where $x = DC_{DA}^{-1/3}t^{2/3}$ and D is diffusion parameter calculated from energy migration microparameter C_{DD} via $D = 0.5(4\pi C_A/3)^{4/3}C_{DD}$. This model is valid in the limit $C_{DD} \ll C_{DA}$. Figure 8c shows a mathematically good fitting quality (R_{adj}^2 = 0.9961). In Table 1, the ET microparameter C_{DA} is fitted to be 4.901 × 10^{-46} m^6/s while the migration microparameter C_{DD} is 10.70 × 10^{-46} m^6/s. These parameters fail to fulfill the validity rule of this model $C_{DD} \ll C_{DA}$, which indicates that the fitting process based on the slow energy migration between Ce^{3+} ions is invalid.

Finally, the Burshteĭn model (hopping model)[40,41] for EDD interaction is applied when a fast energy migration between Ce^{3+} is involved:

$$\frac{I(t)}{I(0)} = \exp\left[-\left(\frac{t}{\tau_0}\right) - \frac{4}{3}\pi^{3/2}C_A(C_{DA})^{1/2}t^{1/2} - Wt\right] \tag{6}$$

where $W = \pi(2\pi/3)^{5/2}C_A^2C_{DA}^{1/2}C_{DD}^{1/2}$. The hopping model is valid in the limit $C_{DA} \ll C_{DD}$. A mathematically good fitting quality (R_{adj}^2 = 0.9962) is presented in Figure 8d, while the obtained ET and migration microparameters in Table 1 still do not satisfy the validity rule of Burshteĭn model. Consequently, the energy transfer between Ce^{3+} to Eu^{2+} is the main process that accelerates the decay of Ce^{3+} excited states, whereas the contributions of energy migration between Ce^{3+} ions in either fast or slow regimes seems negligible.

2.5. X-ray Excited Luminescence of Ce^{3+} and Eu^{2+}.

Figure 9 shows the X-ray excited luminescence spectra of samples BMSO:3% Ce^{3+} and BMSO:2% Eu^{2+} at RT. To estimate their absolute scintillation light yield values under X-ray excitation, the crystal BaF_2 is also measured as a reference at the same condition. For BaF_2 crystal, there are two broad emission bands with the maxima at ~223 and ~317 nm, which are originated to the core valence luminescence and self-trapped-exciton (STE) emission, respectively.[24] For our samples, the profiles and positions of emission bands of Ce^{3+} and Eu^{2+} under X-ray excitation are well consistent with those under VUV–UV excitation discussed above. The peak height of Eu^{2+} emission band is higher than that of reference BaF_2 while the Ce^{3+} emission is much weaker. The absolute scintillation

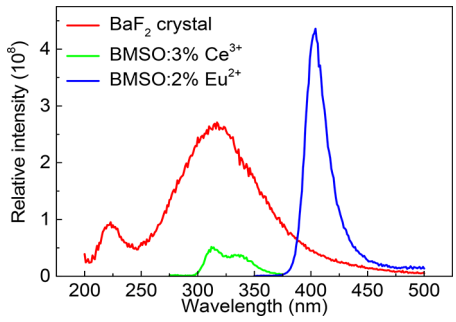

Figure 9. X-ray excited luminescence spectra of samples BMSO:3% Ce^{3+}, BMSO:2% Eu^{2+}, and crystal BaF_2 at RT.

DOI: 10.1021/acs.jpcc.7b12204
J. Phys. Chem. C 2018, 122, 2959–2967

light yields of samples BMSO:3% Ce^{3+} and BMSO:2% Eu^{2+} are further estimated to be ~626 ph·MeV^{-1} and ~3942 ph·MeV^{-1} from the ratio of the integrated intensity of samples with that of BaF_2 (~8880 ph·MeV^{-1}) reference, respectively. Thus, these two materials are not suitable to serve as scintillators for X-ray detection.

3. CONCLUSIONS

In summary, we have systematically studied the host structure, the synchrotron radiation VUV−UV excitation and emission spectra, and the decay properties of samples $BaMg_2Si_2O_7$:Ln (Ce^{3+}, Eu^{2+}) with different doping levels at different temperatures. The Rietveld refinement proves the phase purity of synthesized samples. The mobility band gap of BMSO compound is estimated to be ~8.26 eV, and the centroid shift and crystal field splitting of Ce^{3+} 5d states are ~9.9 × 10^3 cm^{-1} and ~15.9 × 10^3 cm^{-1}, respectively. The doublet emission from the Ce^{3+} lowest 5d excited to 4f ground states $^2F_{5/2}$ and $^2F_{7/2}$ are located at ~32.3 × 10^3 cm^{-1} (~310 nm) and ~30.1 × 10^3 cm^{-1} (~332 nm), respectively. With the increasing of doping concentration, the Ce^{3+} emission shows no quenching in the investigated range. The related temperature-dependent emission spectra imply that Ce^{3+} emission has an excellent thermal stability, which is further confirmed by the energy difference (E_{dc}) between the lowest 5d state and the bottom of conduction band value (~1.40 eV) obtained from the VRBE scheme. The lowest 5d excited state of Eu^{2+} is evaluated to be at ~26.6 × 10^3 cm^{-1} (~376 nm), and it gives a narrow emission peaked at ~396 nm with a full width at half-maximum (fwhm) of ~1.46 × 10^3 cm^{-1} and a small Stokes shift of ~1.37 × 10^3 cm^{-1}. The electron−vibrational interaction (EVI) analysis on Eu^{2+} emission band reveals that the Huang−Rhys factor S = 2.28 and the effective phonon energy $\hbar\omega$ = 384 cm^{-1}, which indicates a weak electron−phonon coupling between Eu^{2+} and the BMSO host. Eu^{2+} doped samples have a quenching concentration of 2 mol %, and the temperature-dependent emission spectra indicate an inferior thermal stability to Ce^{3+} doped samples, which is also confirmed by the VRBE scheme with the E_{dc} value of ~0.55 eV. The energy transfer dynamics from Ce^{3+} to Eu^{2+} was investigated. Three kinetic models were used to study the Ce^{3+} luminescence decay, and the results show that ET from Ce^{3+} to Eu^{2+} via electric dipole−dipole interaction is predominant while the energy migration between Ce^{3+}−Ce^{3+} pairs can be neglected. The ET microparameter C_{DA} is 10.37 × 10^{-46} m^6/s, and the critical distance R_c is about 16.5 Å. Finally, under near-UV 365 nm excitation, Eu^{2+} doped samples are found to possess internal quantum efficiencies (QE) ranging from 58% to 79%. X-ray excited spectra show that BMSO:Ce^{3+} and BMSO:Eu^{2+} are not suitable to serve as scintillators for X-ray detection.

■ ASSOCIATED CONTENT

Supporting Information

The Supporting Information is available free of charge on the ACS Publications website at DOI: 10.1021/acs.jpcc.7b12204.

Experimental details, excitation and emission spectra of Ce^{3+}/Gd^{3+}/Eu^{3+}/Eu^{2+} singly doped samples (Figures S1−S3), the refined structural parameters of compound $BaMg_2Si_2O_7$ at RT (Table S1), the fwhm values (Table S2), and internal quantum yields (Table S3) of Eu^{2+} doped samples (PDF)

■ AUTHOR INFORMATION

Corresponding Author

*E-mail cesbin@mail.sysu.edu.cn; Tel +86-20-84113695 (H.L.).

ORCID

Yiyi Ou: 0000-0002-2111-5064
Weijie Zhou: 0000-0001-5199-9836
Litian Lin: 0000-0003-3241-2651
Hongbin Liang: 0000-0002-3972-2049

Author Contributions

Y.O. and W.Z. contributed equally to this work.

Notes

The authors declare no competing financial interest.

■ ACKNOWLEDGMENTS

The work is financially supported by the National Natural Science Foundation of China (U1432249, 21671201, and U1632101) and the Science and Technology Project of Guangdong Province (2017A010103034). M.G.B. thanks supports from the Program for the Foreign Experts (Contract No. W2017011) and Wenfeng High-end Talents Project (Grant No. W2016-01) offered by Chongqing University of Posts and Telecommunications, China−Poland Intergovernmental Science and Technology Cooperation Program (Grant No. 2015[170]/36-13), Ministry of Education and Research of Estonia, Project PUT430 European Regional Development Fund (project TK141), and Guest Professorship at Kyoto University (Prof. S. Tanabe laboratory).

■ REFERENCES

(1) Pust, P.; Weiler, V.; Hecht, C.; Tücks, A.; Wochnik, A. S.; Henß, A.-K.; Wiechert, D.; Scheu, C.; Schmidt, P. J.; Schnick, W. Narrow-Band Red-Emitting Sr[$LiAl_3N_4$]:Eu^{2+} as a Next-Generation LED-Phosphor Materials. *Nat. Mater.* **2014**, *13*, 891−896.

(2) Dai, P.-P.; Li, C.; Zhang, X.-T.; Xu, J.; Chen, X.; Wang, X.-L.; Jia, Y.; Wang, X. J.; Liu, Y.-C. A Single Eu^{2+}-Activated High-Color-Rendering Oxychloride White-Light Phosphor for White-Light-Emitting Diodes. *Light: Sci. Appl.* **2016**, *5*, e16024.

(3) Wang, Y. C.; Ding, J. Y.; Wang, Y. H. $Ca_{2-x}Y_{1+x}Zr_{2-x}Al_{3+x}O_{12}$:$Ce^{3+}$: Solid Solution Design toward the Green Emission Garnet Structure Phosphor for Near-UV LEDs and Their Luminescence Properties. *J. Phys. Chem. C* **2017**, *121*, 27018−27028.

(4) Li, S. X.; Zhu, Q. Q.; Wang, L.; Tang, D. M.; Cho, Y. J.; Liu, X. J.; Hirosaki, N.; Nishimura, T.; Sekiguchi, T.; Xie, R.-J.; et al. $CaAlSiN_3$:Eu^{2+} Translucent Ceramic: a Promising Robust and Efficient Red Color Converter for Solid State Laser Displays and Lighting. *J. Mater. Chem. C* **2016**, *4*, 8197−8205.

(5) Dorenbos, P. Fundamental Limitation in the Performance of Ce^{3+}-, Pr^{3+}-, and Eu^{2+}- Activated Scintillators. *IEEE Trans. Nucl. Sci.* **2010**, *57*, 1162−1167.

(6) Zhuang, Y. X.; Lv, Y.; Li, Y.; Zhou, T. L.; Xu, J.; Ueda, J.; Tanabe, S.; Xie, R.-J. Study on Trap Levels in $SrSi_2AlO_2N_3$:Eu^{2+},Ln^{3+} Persistent Phosphors Based on Host-Referred Binding Energy Scheme and Thermoluminescence Analysis. *Inorg. Chem.* **2016**, *55*, 11890−11897.

(7) Ueda, J.; Maki, R.; Tanabe, S. Vacuum Referred Binding Energy (VRBE)-Guided Design of Orange Persistent $Ca_3Si_2O_7$:Eu^{2+} Phosphors. *Inorg. Chem.* **2017**, *56*, 10353−10360.

(8) Shi, R.; Xu, J. Z.; Liu, G. K.; Zhang, X. J.; Zhou, W. J.; Pan, F. J.; Huang, Y.; Tao, Y.; Liang, H. B. Spectroscopy and Luminescence Dynamics of Ce^{3+} and Sm^{3+} in $LiYSiO_4$. *J. Phys. Chem. C* **2016**, *120*, 4529−4537.

(9) Liu, G. K. A. Degenerate Model of Vibronic Transitions for Analyzing 4f-5d Spectra. *J. Lumin.* **2014**, *152*, 7−10.

DOI: 10.1021/acs.jpcc.7b12204
J. Phys. Chem. C 2018, 122, 2959−2967

(10) Zhu, Q.-Q.; Wang, L.; Hirosaki, N.; Hao, L. Y.; Xu, X.; Xie, R.-J. Extra-Broad Band Orange-Emitting Ce^{3+}-Doped $Y_3Si_5N_9O$ Phosphor for Solid-State Lighting: Electronic, Crystal Structures and Luminescence Properties. *Chem. Mater.* **2016**, *28*, 4829−4839.
(11) Zhang, X. J.; Fang, M.-H.; Tsai, Y.-T.; Lazarowska, A.; Mahlik, S.; Lesniewski, T.; Grinberg, M.; Pang, W. K.; Pan, F. J.; Liu, R. S.; et al. Controlling of Structural Ordering and Rigidity of β-SiAlON: Eu through Chemical Cosubstitution to Approach Narrow-Band-Emission for Light-Emitting Diodes Application. *Chem. Mater.* **2017**, *29*, 6781−6792.
(12) Zhang, Y.; Geng, D. L.; Li, X. J.; Fan, J.; Li, K.; Lian, H. Z.; Shang, M. M.; Lin, J. Wide-Band Excited $YTiTaO_6$:Eu^{3+}/Er^{3+} Phosphors: Structure Refinement, Luminescence Properties, and Energy Transfer Mechanisms. *J. Phys. Chem. C* **2014**, *118*, 17983−17991.
(13) Liu, X. M.; Lü, Y.; Chen, C.; Luo, S. L.; Zeng, Y. H.; Zhang, X. Q.; Shang, M. M.; Li, C. X.; Lin, J. Synthesis and Luminescence Properties of $YNbO_4$:A (A = Eu^{3+} and/or Tb^{3+}) Nanocrystalline Phosphors via a Sol-Gel Process. *J. Phys. Chem. C* **2014**, *118*, 27516−27524.
(14) Zhou, W. J.; Gu, M.; Ou, Y. Y.; Zhang, C. H.; Zhang, X. J.; Zhou, L.; Liang, H. B. Concentration-Driven Selectivity of Energy Transfer Channels and Color Tunability in $Ba_3La(PO_4)_3$:Tb^{3+},Sm^{3+} for Warm White LEDs. *Inorg. Chem.* **2017**, *56*, 7433−7442.
(15) Shannon, R. D. Revised Effective Ionic Radii and Systematic Studies of Interatomic Distances in Halides and Chalcogenides. *Acta Crystallogr., Sect. A: Cryst. Phys., Diffr., Theor. Gen. Crystallogr.* **1976**, *32*, 751−767.
(16) Dorenbos, P. The Eu^{3+} Charge Transfer Energy and the Relation with the Band Gap of Compounds. *J. Lumin.* **2005**, *111*, 89−104.
(17) Fan, L. C.; Lin, D. B.; Zhang, X. X.; Shi, Y.; Zhang, J. Y.; Xie, J. J.; Lei, F.; Zhang, L. Local Structures of Lu Atoms in a Core-Shell Approach for Synthesis of Lu_2SiO_5 Phase. *Chem. Phys. Lett.* **2016**, *644*, 41−44.
(18) Zhang, Z. Y.; Wang, Y. H. UV-VUV Excitation Luminescence Properties of Eu^{2+}-Doped $Ba_2MSi_2O_7$ (M = Mg, Zn). *J. Electrochem. Soc.* **2007**, *154*, J62−J64.
(19) Lin, H. H.; Liang, H. B.; Han, B.; Zhong, J. P.; Su, Q.; et al. Luminescence and Site Occupancy of Ce^{3+} in $Ba_2Ca(BO_3)_2$. *Phys. Rev. B: Condens. Matter Mater. Phys.* **2007**, *76*, 035117.
(20) Dorenbos, P. 5d-Level Energies of Ce^{3+} and the Crystalline Environment. III. Oxides Containing Ionic Complexes. *Phys. Rev. B: Condens. Matter Mater. Phys.* **2001**, *64*, 125117−125128.
(21) Dorenbos, P.; Pierron, L.; Dinca, L.; van Eijk, C. W. E.; Kahn−Harari, A.; Viana, B. 4f-5d Spectroscopy of Ce^{3+} in $CaBPO_5$, $LiCaPO_4$ and Li_2CaSiO_4. *J. Phys.: Condens. Matter* **2003**, *15*, 511−520.
(22) Guo, C. F.; Xu, Y.; Ren, Z. Y.; Bai, J. T. Blue-White-Yellow Tunable Emission from Ce^{3+} and Eu^{2+} Co-Doped $BaSiO_3$ Phosphor. *J. Electrochem. Soc.* **2011**, *158*, J373−J376.
(23) Yan, J.; Liu, C. M.; Zhou, W. J.; Huang, Y.; Tao, Y.; Liang, H. B. VUV-UV-Vis Photoluminescence of Ce^{3+} and Ce^{3+}-Eu^{2+} Energy Transfer in $Ba_2MgSi_2O_7$. *J. Lumin.* **2017**, *185*, 251−257.
(24) Liu, C. M.; Qi, Z. M.; Ma, C. G.; Dorenbos, P.; Hou, D. J.; Zhang, S.; Kuang, X. J.; Zhang, J. H.; Liang, H. B. High Light Yield of $Sr_8(Si_4O_{12})Cl_8$:Eu^{2+} under X-ray Excitation and Its Temperature-Dependent Luminescence Characteristics. *Chem. Mater.* **2014**, *26*, 3709−3715.
(25) Dorenbos, P. Thermal Quenching of Eu^{2+} 5d-4f Luminescence in Inorganic Compounds. *J. Phys.: Condens. Matter* **2005**, *17*, 8103−8111.
(26) Dorenbos, P. Ce^{3+} 5d-Centroid Shift and Vacuum Referred 4f-Electron Binding Energies of All Lanthanide Impurities in 150 Different Compounds. *J. Lumin.* **2013**, *135*, 93−104.
(27) Dorenbos, P. A Review on How Lanthanide Impurity Levels Change with Chemistry and Structure of Inorganic Compounds. *ECS J. Solid State Sci. Technol.* **2013**, *2*, R3001−R3011.
(28) Luo, H. D.; Bos, A. J. J.; Dobrowolska, A.; Dorenbos, P. Low−Temperature VUV Photoluminescence and Thermoluminescence of UV Excited Afterglow Phosphor Sr3AlxSi1-xO5:Ce3+, Ln3+ (Ln = Er, Nd, Sm, Dy and Tm). *Phys. Chem. Chem. Phys.* **2015**, *17*, 15419−15427.
(29) Lin, L. T.; Shi, R.; Zhou, R. F.; Peng, Q.; Liu, C. M.; Tao, Y.; Huang, Y.; Dorenbos, P.; Liang, H. B. The Effect of Sr^{2+} on Luminescence of Ce^{3+}-Doped $(Ca, Sr)_2Al_2SiO_7$. *Inorg. Chem.* **2017**, *56*, 12476−12484.
(30) Zhang, X. J.; Tsai, Y. T.; Wu, S. M.; Lin, Y. C.; Lee, J. F.; Sheu, H. S.; Cheng, B. M.; Liu, R. S. Facile Atmospheric Pressure Synthesis of High Thermal Stability and Narrow-Band Red-Emitting $SrLiAl_3N_4$:Eu^{2+} Phosphors for High Color Rendering Index White Light-Emitting Diodes. *ACS Appl. Mater. Interfaces* **2016**, *8*, 19612−19617.
(31) Ye, S.; Zhang, J. H.; Zhang, X.; Lu, S. Z.; Ren, X. G.; Wang, X. J. Mn^{2+} Concentration Manipulated Red Emission in $BaMg_2Si_2O_7$:Eu^{2+}, Mn^{2+}. *J. Appl. Phys.* **2007**, *101*, 033513.
(32) Nazarov, M.; Tsukerblat, B.; Noh, D. Y. Vibronic Coupling Parameters and Stokes Shift in Thiogallate Phosphors. *J. Phys. Chem. Solids* **2008**, *69*, 2605−2612.
(33) Henderson, B.; Imbusch, G. F. *Optical Spectroscopy of Inorganic Solids*; Oxford University Press: 2006.
(34) Park, C.-H.; Choi, Y.-N. Crystal Structure of $BaMg_2Si_2O_7$ and Eu^{2+} Luminescence. *J. Solid State Chem.* **2009**, *182*, 1884−1888.
(35) Hou, D. J.; Ma, C.-G.; Liang, H. B.; Brik, M. G. Electron-Vibrational Interaction in the 5d States of Eu^{2+} Ions in $Sr_{6-x}Eu_xBP_5O_{20}$ (x = 0.01 − 0.15). *ECS J. Solid State Sci. Technol.* **2014**, *3*, R39−R42.
(36) Ji, H. P.; Huang, Z. H.; Xia, Z. G.; Molokeev, M. S.; Atuchin, V. V.; Fang, M. H.; Huang, S. F. New Yellow-Emitting Whitlockite-Type Structure $Sr_{1.75}Ca_{1.25}(PO_4)_2$:$Eu^{2+}$ Phosphor for Near-UV Pumped White Light-Emitting Devices. *Inorg. Chem.* **2014**, *53*, 5129−5135.
(37) Wang, C.-Y.; Takeda, T.; Kate, O. M. T.; Tansho, M.; Deguchi, K.; Takahashi, K.; Xie, R.-J.; Shimizu, T.; Hirosaki, N. Ce-Doped $La_3Si_{6.5}Al_{1.5}N_{9.5}O_{5.5}$, a Rare Highly Efficient Blue-Emitting Phosphor at Short Wavelength toward High Color Rendering White LED Application. *ACS Appl. Mater. Interfaces* **2017**, *9*, 22665−22675.
(38) Inokuti, M.; Hirayama, F. Influence of Energy Transfer by the Exchange Mechanism on Donor Luminescence. *J. Chem. Phys.* **1965**, *43*, 1978−1989.
(39) Yokota, M.; Tanimoto, O. Effects of Diffusion on Energy Transfer by Resonance. *J. Phys. Soc. Jpn.* **1967**, *22*, 779−784.
(40) Georgescu, S.; Voiculescu, A. M.; Matei, C.; Stefan, A.; Toma, O.; Birjega, R. Upconversion Luminescence in Langatate Ceramics Doped with Tm^{3+} and Yb^{3+}. *J. Lumin.* **2014**, *154*, 74−79.
(41) Burshtein, A. I. The Influence of the Migration Mechanism of Approaching Particles on the Energy Transfer Between Them. *J. Lumin.* **1980**, *21*, 317−321.

DOI: 10.1021/acs.jpcc.7b12204
J. Phys. Chem. C 2018, 122, 2959−2967